Contents lists available at ScienceDirect

Journal of Hydrology

journal homepage: http://ees.elsevier.com

Research papers

Improved prediction of water retention curves for fine texture soils using an intergranular mixing particle size distribution model

J.A.P. Pollacco, J. Fernández-Gálvez [1,*], S. Carrick

Manaaki Whenua – Landcare Research, Lincoln 7640, New Zealand

ARTICLE INFO

This manuscript was handled by Corrado Corradini, Editor-in-Chief, with the assistance of Renato Morbidelli, Associate Editor

Keywords
Particle size distribution
Pore size distribution
Water retention curve
Intergranular mixing
Kosugi model

ABSTRACT

Laboratory measurements to derive the soil water retention curve, $\theta(\psi)$, are time consuming and expensive. We present a cost-effective alternative using particle size distribution (PSD) and saturated water content. We propose a novel physical conceptual intergranular mixing PSD model (IMP model) which derives $\theta(\psi)$ from PSD, exploiting the relation between particle size and pore size distributions and the intergranular arrangement of the soil particles. The IMP model successfully predicts $\theta(\psi)$ for fine texture soil, which is the most challenging soil texture to be modelled. With our novel model, reliable $\theta(\psi)$ can be obtained using only three general fitting parameters without needing to assume any particular type of soil particle packing, with mean Nash–Sutcliffe efficiency coefficient of 0.92 for 259 soils. The IMP model can accurately predict $\theta(\psi)$ for fine texture soils because: a) it implements an intergranular mixing function that accounts for soil pores not all being perfectly spherical and takes into consideration the intergranular rearrangement (mixing) of the particles, which allows neighbouring particles to have different sizes resulting in variations in pore radius and pore shape of the corresponding pore fraction; b) it overcomes the absence of PSD data for sizes smaller than the clay fraction by developing a normalised form of the Young–Laplace capillary equation; and c) the residual pore volume accounting for water strongly bound to solid particles or in very small pores is incorporated as a function of the clay fraction.

1. Introduction

The soil water retention curve, $\theta(\psi)$, is fundamental in describing the storage and transmission of water in the soil. The $\theta(\psi)$ relates the soil water content, θ [L^3 L^{-3}], to the soil matric potential or suction, ψ [L], in a distinct relationship for different soils. The $\theta(\psi)$ is experimentally determined by measuring the amount of water that remains in the soil at a certain suction. Measurements normally range between saturation and permanent wilting point 1500 kPa. Because laboratory measurements are time consuming and expensive, estimations of the $\theta(\psi)$ can alternatively be derived from soil physical properties. Different approaches include directly estimating points from the $\theta(\psi)$ (e.g. Balland and Pollacco, 2008; Pollacco, 2008) or estimating the whole $\theta(\psi)$ curve using empirical pedotransfer functions (McNeill et al., 2018; van Looy et al., 2017) derived from surrogate soil measurements.

One promising approach is to derive the $\theta(\psi)$ curve from the soil particle size distribution (PSD), based on the similarity between the *cumulative particle size distribution*, $\sum PSD$, and the *cumulative pore size distribution*, $\sum PoreSD$. The latter corresponds to $\theta(\psi)$ (e.g. Arya and Paris, 1981; Chang et al., 2019; Mohammadi and Vanclooster, 2011; Nasta et al., 2013).

PSD is a fundamental soil physical characteristic used for soil classification and for the estimation of other physical properties such as hydraulic and thermal characteristics (Yang et al., 2019). The routinely-used sieve and sediment method for measuring PSD separates larger particle fractions by wet-sieving, then smaller particle fractions by sedimentation (Klute, 1986) and assumes sphericity of the individual soil particles and a constant particle density for all size ranges.

Arya and Paris (1981) developed the first conceptual model to derive $\theta(\psi)$ from PSD using a semi-physical approach in which pore size was associated with pore volume and determined by scaling the pore length. Pore lengths based on spherical particles were scaled using an empirical scaling parameter. Further formulations of this empirical scaling parameter have been proposed to improve the prediction of the $\theta(\psi)$ (Arya et al., 2008). Alternative semi-physical models have been proposed using empirical parameters and specific assumptions relating to the relationship between particle size and pore size. Nevertheless, these approaches fail to predict $\theta(\psi)$ from PSD for loamy and fine tex-

* Corresponding author.
E-mail address: jesusfg@ugr.es (J. Fernández-Gálvez)
[1] Permanent address: Department of Regional Geographic Analysis and Physical Geography, University of Granada, Spain.

https://doi.org/10.1016/j.jhydrol.2020.124597
Received 2 October 2019; Received in revised form 14 January 2020; Accepted 16 January 2020
Available online xxx
0022-1694/

ture soils (e.g. Haverkamp and Parlange, 1986; Zhuang et al., 2001; Nimmo et al., 2007; Mohammadi and Vanclooster, 2011; Chang et al., 2019).

To relate $\sum PSD$ to $\sum PoreSD$ and its corresponding $\theta(\psi)$, Mohammadi and Vanclooster (2011) presented a simple physical-empirical conceptual model to retrieve the $\theta(\psi)$ from PSD. The soil is described as an ensemble of particles of different sizes where, for each particle size, the void ratio (the ratio of volume of voids to the volume of solids) is related to particle size and the type of packing of the soil particles. The size of the particle is related to the effective pore size that forms between the particles, and the integration over all particle sizes then allows calculation of $\sum PoreSD$ as a function of $\sum PSD$. Several types of packing were considered, including *close-packed cubic, cubical tetrahedral, tetragonal spheroidal, pyramidal, tetrahedral, and body-centred cubic*. Finally, pore size is related to ψ through the Young-Laplace capillary equation to provide $\theta(\psi)$.

However, in their approach, Mohammadi and Vanclooster (2011) assumed the same type of packing for all particle sizes, making the void ratio constant regardless of particle size. This is a common assumption (e.g. Arya and Paris, 1981) that simplifies the derivation of the $\theta(\psi)$ when linking $\sum PSD$ to the equivalent $\sum PoreSD$, since the ratio between particle size and pore size is constant when the geometry of the pores is considered similar to the geometry of the particles. However, in a soil the geometry of the pores can vary with the size of the particles, leading to a variable relationship between the particle radius and pore radius.

The purpose of this study is to develop a model that can account for the possibility of a pore system formed by neighbours' particles of different sizes. In this study, we hypothesize that the geometry of the pores depends on the size of the soil particles and the intergranular mixing between particles of different sizes. The intergranular mixing accounts for the organisation of neighbouring soil particles of different sizes. We therefore propose an intergranular mixing PSD (IMP) model. We revisit the conceptual model of Mohammadi and Vanclooster (2011), considering the intergranular mixing of particle sizes, and propose an expression to account for it. The predicted $\theta(\psi)$ from a set of PSD data points using the traditional sieve and sediment method is compared to the $\theta(\psi)$ from laboratory data using the drying curve. The proposed model is compared with the recent Chang et al. (2019) model, which is currently one the models providing better agreement between $\theta(\psi)$ from laboratory data and predicted $\theta(\psi)$ from PSD. This model outperforms that of Meskini-Vishkaee et al. (2014), a modification of the Mohammadi and Vanclooster (2011) model that improved it by including a soil particle scaling factor.

The manuscript is organised as follows: Section 2 outlines the theory behind the proposed model, briefly describes the model used for comparison, and the fundamental physical approach on which our intergranular mixing approach is based; Section 3 presents the experimental data and the numerical computations used to derive $\theta(\psi)$ from the laboratory measurements and from the IMP model; Section 4 evaluates the model performance and illustrates the relevance of the processes considered; and Section 5 summarises the key conclusions.

2. Theory

The $\sum PSD$ is divided into m fractions, depending on the measurement method or available data. The mass ratio and the representative particle radius for the i-th fraction are w_i [M M^{-1}] and R_i [L] respectively ($i \leq m$). Solid particles within each fraction are packed considering uniform-sized spherical particles with the same bulk density as the soil.

As proposed by Arya and Paris (1981), the volumetric water content θ_i [L^3 L^{-3}] is obtained by summation of pore volumes that progressively fill up with water from the smallest fraction to the corresponding soil water content. The $\sum PSD$ is used to compute θ_i by multiplying the saturated soil water content, θ_s [L^3 L^{-3}], by the cumulative mass ratio of particles up to the i-th fraction:

$$\theta_i = \theta_s \sum_{j=1}^{i} w_j \tag{1}$$

where θ_s is the saturated soil water content and w_i is the mass ratio which represents the particle radius for the i-th fraction, R_i ($i \leq m$).

The determination of the $\theta(\psi)$ relies on the fact that for a given matric potential, ψ_i [L], only part of the pore fractions are activated. This activation is ruled by the Young-Laplace capillary equation, which takes the following general form (Tuller et al., 1999):

$$\psi_i = \frac{C_i}{A_i} \frac{\gamma \cos\Theta}{\rho_w g} \tag{2}$$

where ρ_w[M L^{-3}] is the density of water, g[L T^{-2}] is the acceleration due to gravity, C_i [L] and A_i [L^2] correspond respectively to the circumference and the cross-sectional area of the narrowest part of the pore for the corresponding fraction, γ [M T^{-2}] is the surface tension at the air–water interface, and Θ [°] is the contact angle between the soil particle and the water. The ratio A_i/C_i has the dimension of a length and equals $r_i/2$ for a perfectly cylindrical pore of radius r_i [L]. Therefore, the Young–Laplace capillary equation is written as:

$$\psi_i = \frac{2\gamma \cos\Theta}{\rho_w g\, r_i} = \frac{Y}{r_i} \tag{3}$$

where Y equals 14.9 mm^2 for pure water at 20 °C and a contact angle of 0° ($\gamma = 0.0728$ kg s^{-2}, $\rho_w = 998.2067$ kg m^{-3}, and $g = 9.8067$ m s^{-2}).

2.1. Chang et al. (2019) *model*

When Eq. (1) is used to compute the cumulative pore volume, the residual pore fraction is greater than the corresponding clay fraction. This is notable for small particle sizes that become embedded within the pores formed by the larger particles, increasing the pore volume formed by the smaller particles (which are protected from compaction) and reducing the pore volume fraction associated with large particles, filling up the space of bigger pores by small particles (Fernández-Gálvez and Barahona, 2005).

To account for the increase in the pore volume by the smallest particle size (corresponding to the clay fraction), Chang et al. (2019) introduced an empirical relationship derived for a range of contrasting soil textures taken from the UNSODA database:

$$\begin{cases} \theta_1 = \theta_s Clay^{\eta} & \text{with } \eta \text{ optimised} \\ \theta_i = \theta_1 + \theta_s \sum_{j=2}^{i} \left(w_i - (Clay^{\eta} - Clay) \frac{w_i}{\sum_{j=2}^{m} w_j} \right) & \text{for } i > 1 \end{cases} \tag{4}$$

where η [–] is a fitting parameter (found equal to 0.516), θ_1 [L^3 L^{-3}] is the residual pore fraction and *Clay* [M M^{-1}] refers to the percentage of the clay fraction. To relate pore radius, r, to ψ, Chang et al. (2019) used a linear relationship between r and associated particle radius, R, using the scale factor of 0.3 as indicated here:

$$\psi_i = \frac{Y}{0.3 R_i} \tag{5}$$

Although Chang et al. (2019) improved estimates of $\theta(\psi)$ compared to the Mohammadi and Vanclooster (2011) model and its scaled version (Meskini-Vishkaee et al., 2014) specifically developed for the van Genuchten (1980) hydraulic model, it still shows poor predictions for silty soils, which we will address in this paper.

2.2. Mohammadi and Vanclooster (2011) *model*

For each particle fraction, w_i, with a representative particle radius, R_i, the assemblage of these particles forms a pore fraction for which the pore radius, r_i, can be geometrically related to the particle radius. In a close-packed cubic assemblage for a particle radius R_i, where eight spherical particles contribute to each assembly, the pore volume for a single assembly is the total volume of the assembly, $(4R_i)^3$, minus the solid volume of the corresponding spherical particles, $8\left(4\pi R_i^3\right)/3$. This assumption implies that neighbouring particles are of similar size within each particle fraction.

To account for alternative structures where the number of spherical particles contributing to a single assembly differs from eight, Mohammadi and Vanclooster (2011) introduced a coefficient that depends on the state of packing, P_{state}. Therefore, the void ratio, e [−], of the assemblage takes the following form:

$$e = \frac{(4R_i)^3 - 8P_{state}\left(4\pi R_i^3\right)/3}{8P_{state}\left(4\pi R_i^3\right)/3} = \frac{6 - \pi P_{state}}{\pi P_{state}} \tag{6}$$

Then,

$$P_{state} = \frac{6}{\pi(1+e)} = \frac{6}{\pi}(1-\phi) \tag{7}$$

where ϕ [−] is the total porosity and e [−] is the void ratio which relates to the solid particle density, ρ_s [M L^{-3}], and the soil bulk density, ρ_b [M L^{-3}], by:

$$e = \frac{\rho_s - \rho_b}{\rho_b} \tag{8}$$

Mohammadi and Vanclooster (2011) assumed that for soil particles in the *i*-th size fraction, particularly for a close-packed cubic assemblage with uniform-size spherical particles of radius R_i, the ratio C_i/A_i is:

$$\frac{C_i}{A_i} = \frac{2\pi R_i P_{state}}{(2R_i)^2 - \left(\pi R_i^2\right)} = \frac{2\pi P_{state}}{(4-\pi)R_i} \tag{9}$$

For other types of soil particle packing, the ratio can be written in its general form as:

$$\frac{C_i}{A_i} = \frac{P_{type}P_{state}}{R_i} \tag{10}$$

where P_{type} [−] describes the packing type, which Mohammadi and Vanclooster (2011) found to have an average value of 7.3, corresponding to close-packed cubic packing. P_{type} can vary between 2.866 and 19.470, depending on the geometric characteristics of the packing of the soil particles, which are assumed to be spherical. Different particle size fractions may have different types of packing, which then modifies the number of spherical particles devoted to each assemblage.

Mohammadi and Vanclooster (2011) compute Ψ for a general pore with cross-section shape in the soil by:

$$\begin{aligned}\psi_i &= \frac{P_{state}P_{type}}{R_i}\frac{\gamma\cos\Theta}{\rho_w g} \\ &= \frac{P_{state}P_{type}Y}{2R_i} \\ &= \frac{3(1-\phi)P_{type}Y}{\pi R_i}\end{aligned} \tag{11}$$

Considering Eq. (3), this leads to the following relation between particle radius, R_i, and pore radius, r_i:

$$r_i = \frac{2R_i}{P_{state}P_{type}} = \frac{\pi R_i}{3(1-\phi)P_{type}} \tag{12}$$

Eq. (5) is similar to Eq. (11) with similar scale factors when P_{type} corresponds to the close-packed cubic packing.

2.3. Novel model to predict $\theta(\psi)$ from PSD

Using principles of soil physics, the uncertainty associated with the packing type is eliminated by constraining the total volume of spherical pores to the soil water content at saturation, θ_s. The maximum amount of water in the soil system for perfectly spherical pores ($\xi = 0$) can be calculated from the sum of all pore volumes up to the maximum pore size using the following expression:

$$\theta_s = \frac{4\pi}{3}\sum_{j=1}^{m} n_j r_j^{3-\xi} \tag{13}$$

where n_j [M^{-1}] is the number of spherical pores for each fraction of the pore size distribution and ξ [−], with values in the range [0–3[, accounts for soil pores not all being perfectly spherical (ξ is further discussed in Section 2.3.1). For the limiting case when $\xi = 0$, the pores are perfectly spherical (Pollacco et al., 2017, 2013) and neighbouring particles are of similar size (Mohammadi and Vanclooster 2011).

The number of spherical pores for each pore fraction is assumed to be equal to the number of spherical particles for each fraction, which is corrected by ξ, and therefore calculated dividing the mass ratio by the total mass of the corresponding fraction:

$$n_j = \frac{3w_j}{4\pi\rho_s R_j^3} \tag{14}$$

where for the calculation of n_j for each R_j it is assumed that ρ_s is equal for all particle sizes.

Combining Eq. (13) with (12) and (14) gives:

$$\theta_s = \frac{1}{\rho_s}\left(\frac{\pi}{3(1-\phi)P_{type}}\right)^{3-\xi}\sum_{j=1}^{m} w_j R_j^{-\xi} \tag{15}$$

from where P_{type} can be isolated:

$$P_{type} = \frac{\pi}{3(1-\phi)}\left(\frac{1}{\theta_s\rho_s}\sum_{j=1}^{m} w_j R_j^{-\xi}\right)^{\frac{1}{3-\xi}} \tag{16}$$

The soil water content of the *i*-th fraction, θ_i, can be obtained from successive summations corresponding to particle radius up to *i*-th, as for the total volume of pores in Eq. (13):

$$\theta_i = \frac{4\pi}{3}\sum_{j=1}^{i} n_j r_j^{3-\xi} \tag{17}$$

Replacing r_i by R_i using Eq. (12), substituting n_i from Eq. (14), and P_{type} from Eq. (16) leads to:

$$\theta_i = \theta_s\frac{\sum_{j=1}^{i} w_j R_j^{-\xi}}{\sum_{j=1}^{m} w_j R_j^{-\xi}} \tag{18}$$

When $\xi = 0$, this expression reduces to Eq. (1).

Standard PSD measurements lack data below 0.001 mm effective radius, limiting the practicality of deriving θ in dry conditions (high Ψ). The residual particle size fraction that accounts for the contribution

of the residual soil water content, $\theta_{r\ psd}$ [$L^3\ L^{-3}$], is limited by the smallest measured particle fraction, which can be related to the clay fraction (e.g. Pollacco et al., 2008b; Chang et al., 2019). Therefore, for a better estimation of the soil water content the expression is modified to:

$$\theta_i = \left(\theta_s - \theta_{r\ psd}\right) \frac{\sum_{j=1}^{i} w_j R_j^{-\xi}}{\sum_{j=1}^{m} w_j R_j^{-\xi}} + \theta_{r\ psd} \tag{19}$$

The relationship between $\theta_{r\ psd}$ and the soil clay fraction is described in Section 2.3.2.

The soil matric potential corresponding to particle radius up to the i-th fraction, Ψ_i, is described by Chang et al. (2019) and Mohammadi and Vanclooster (2011) in the form of the Young–Laplace capillary equation using quite similar scale factors as those in Eqs. (5) and (11), respectively. Because routine methods cannot measure particle sizes smaller than the clay fraction, expressions based on the Young–Laplace capillary equation fail to describe Ψ for pore fractions corresponding to smaller particles assemblages as shown in Fig. 1. For example, for R_{Min} = 0.001 mm gives Ψ = 500 kPa, which does not take into account the large suction corresponding to the very small pores. Therefore, an alternative normalized expression of the Young–Laplace capillary equation is proposed, in which a linear relation between pore radius and particle radius is considered:

$$\begin{aligned}\Psi_i &= \Psi_{Max} \cdot \left(\frac{\frac{Y}{r_i} - \frac{Y}{r_{Max}}}{\frac{Y}{r_{Min}} - \frac{Y}{r_{Max}}} \right)^{\lambda} \\ &= \Psi_{Max} \cdot \left(\frac{\frac{3(1-\phi)P_{type}Y}{\pi R_i} - \frac{3(1-\phi)P_{type}Y}{\pi R_{Max}}}{\frac{3(1-\phi)P_{type}Y}{\pi R_{Min}} - \frac{3(1-\phi)P_{type}Y}{\pi R_{Max}}} \right)^{\lambda} \\ &= \Psi_{Max} \cdot \left(\frac{\frac{1}{R_i} - \frac{1}{R_{Max}}}{\frac{1}{R_{Min}} - \frac{1}{R_{Max}}} \right)^{\lambda}\end{aligned} \tag{20}$$

where Ψ_{Max} represents the maximum value of the matric potential, which corresponds to a value marginally larger than wilting point and is set to 1600 kPa to account for the feasible range of matric potential; Y from Eq. (3) corresponds to the constant in the Young-Laplace capillary equation (14.9 mm^2); r_{Max} and r_{Min} are the maximum and minimum pore radius; R_{Max} and R_{Min} are the maximum and minimum particle radius determined experimentally; and λ is a shape parameter to account for the fact that the correction for Ψ only applies for the smaller particles.

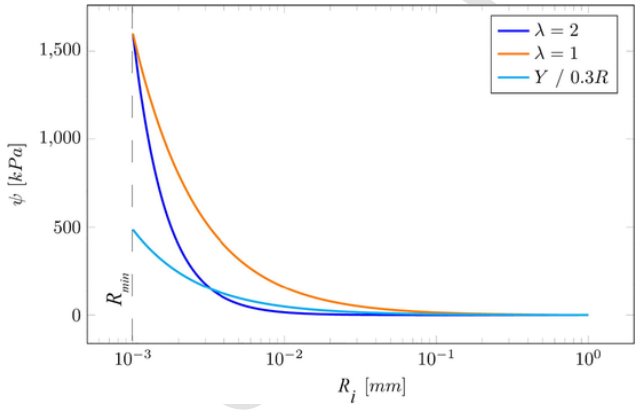

Fig. 1. Soil matric potential as a function of soil particle radius as in Eq. (20) with Ψ_{Max} set to 1600 kPa for λ equals 1 (blue), λ equals 2 (orange), and by the classic approximation using the Young-Laplace equation (cyan) as in Chang et al. (2019). (For interpretation of the references to colour in this figure legend, the reader is referred to the web version of this article.)

Fig. 1 compares different expressions that relate Ψ to R based on the Young–Laplace capillary equation used by Chang et al. (2019) (Eq. (5)) and the normalized form (Eq. (20)) for cases when λ equals 1 and 2. R_{Min} corresponds to the clay particle size with an effective radius below 0.001 mm. The proposed normalized expression differs from the classic approximation at smaller particle sizes. For λ = 1 differences can be seen from the very fine sand fraction (particle radius below 0.1 mm), while for λ = 2 the curves start to diverge from the very fine silt fraction (particle radius below 0.003 mm), which gives a better physical description of Ψ such that at R_{Min} = 0.001 mm then Ψ = 1500 kPa.

2.3.1. Novel intergranular mixing function from PSD

As previously indicated, ξ in Eq. (19) is interpreted as a correction to account for the fact that not all soil pores are perfectly spherical. We modify ξ such that it could be interpreted as an *intergranular mixing* function that accounts not only for the non-spherical shape of the soil pores but also for the intergranular rearrangement (mixing) of the particles in a soil. Therefore, we hypothesise that ξ could be expressed as a function of effective R_i using the following expression, which is introduced into Eq. (19):

$$\xi\left(R_i\right) = \xi_1 \exp\left(-R_i^{-\xi_2}\right) \tag{21}$$

where ξ_1 [−] and ξ_2 [−] are intergranular mixing parameters to account for intergranular mixing of the particles depending on their effective size. Pores formed between particles may be of different sizes; we consider that small pores are surrounded by small particles and larger pores are surrounded by large particles, while medium size pores consist of a mixture of small and large particles.

To illustrate this concept, Fig. 2 plots $R_i^{-\xi(R_i)}$ as a function of R_i, where $R_i^{-\xi(R_i)}$ is the weighting function applied to w_i in Eq. (19) as a function of R_i for optimal values of ξ_1 and ξ_2. The bell shape results in larger corrections for moderate particle sizes (in Fig. 2, at around 0.02 mm). Moderate-sized particles result from a mixed size range of particles (polydisperse), decreasing the passages of the pore system (Pollacco et al., 2013, 2017), and therefore requiring a higher suction for the water to be drained, with a consequent higher correction. The arrangement of the soil particles in a unit volume can have neighbouring particles of different sizes, which results in variations in pore radius and pore shape of the corresponding pore fraction.

The bell shape can be shifted depending on the degree of mixing (Fig. 2), where increasing smaller particles in a "polydisperse soil" results in higher mixing. When the amount of smaller particles in-

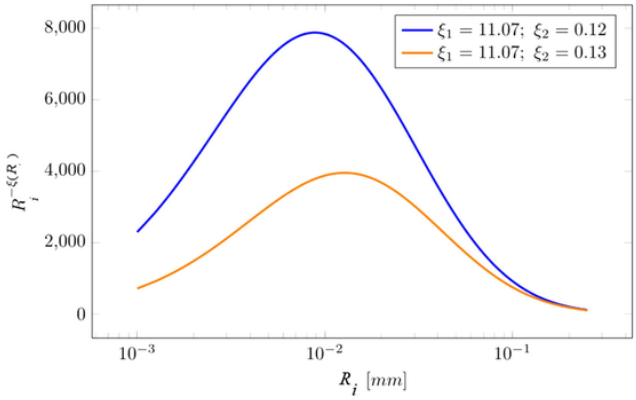

Fig. 2. Theoretical shape of the weighting for the $\sum PSD$, using the intergranular mixing function to transform PSD into $\theta(\psi)$, as a function of particle radius (Eq. (21)) for optimal values of ξ_1 and ξ_2 (blue) and by increasing ξ_2 (orange). (For interpretation of the references to colour in this figure legend, the reader is referred to the web version of this article.)

creases, the correction spreads to a wider range of larger particles (that is, the width of the bell increases). In order to take this effect into account, we vary ξ_2 based on the PSD using the following proposed expression:

$$\xi_2 = \beta_1 \exp\left(\beta_2 \sum_{i=1}^{p} w_i\right) \quad (22)$$

where β_1 [−] and β_2 [−] are two additional fitting parameters and p is a particle distribution fraction that is selected such that ξ_2 is correlated to the optimal ξ_2 derived for individual soils.

2.3.2. Deriving θ_r from PSD

The residual soil water content, θ_r [L^3L^{-3}], is a parameter indicating the amount of water left in the soil at relatively high suction. It can be derived as a fitting parameter from the $\theta(\psi)$. Fixing θ_r to a constant value close to zero results in significant errors in the estimation of $\theta(\psi)$, especially for soils with significant clay fraction (e.g. Lee and Ro, 2014; Mohammadi and Meskini-Vishkaee, 2013). Therefore, predicting θ_r from PSD is required.

For the estimation of θ_r, and subsequently a better prediction of the $\theta(\psi)$, a relationship between the residual pore fraction and clay content is derived as follows:

$$\theta_{r\ psd} = \theta_{r\_max}\ \left(1 - \exp\left(-\alpha_1 \cdot Clay^{\alpha_2}\right)\right) \quad (23)$$

where θ_{r_max} is the maximum value allowed for θ_r that was found to be satisfactory when set at 0.25, and α_1 [-] and α_2 [-] are two empirical parameters. This is described in Fig. 3.

3. Material and methods

3.1. Experimental data

3.1.1. Sites, soils, and profiles description

Soil samples (n = 259) corresponding to 46 soil profiles were collected in Canterbury, New Zealand. Sampled sites included irrigated and non-irrigated pastoral farming land, mostly grazed by dairy cattle, but including mixed sheep and cattle grazed pastures. Rainfall across the sites varied from 550 to 800 mm per year. Soil parent material was sediments derived from quartzo-feldspathic hard sandstone, deposited as either river alluvium or windblown loess (Landcare Research, 2019; Schmidt et al., 2005). Previous research has shown these sediments to have a relatively consistent mineralogy across the region, with the sand fraction dominated by quartz and feldspar, and the clay fraction by mica and chlorite (Bruce, 1984; Rijkse, 1985). This relatively consistent parent material across the sample set is an advantage for develop the theory underpinning the IMP model, because it minimizes the possible complex effects of contrasting mineralogy on the soil hydraulic functions, as well the effects of more complex mineralogy on the reliability of laboratory measurements, such as shrink-swell clays or amorphous volcanic minerals (Allbrook, 1993; McNeill et al., 2018). Although beyond the scope of this paper, the IMP approach taken here should be adaptable to account for the effects of different mineralogy on pore geometry, because it explicitly incorporates the effects of intergranular mixing of particles of different sizes.

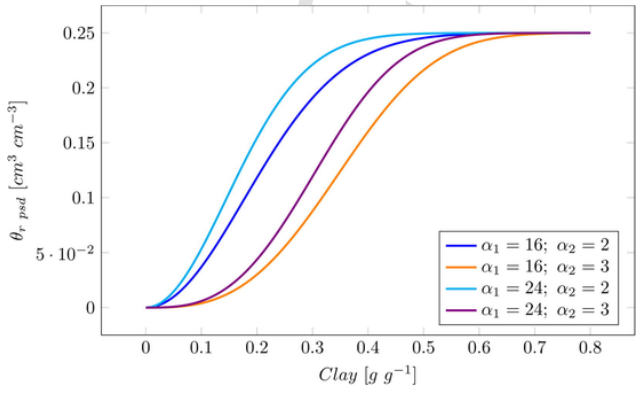

Fig. 3. Theoretical shape of the model corresponding to $\theta_{r\ psd}$ as a function of the soil clay fraction as in Eq. (23) with θ_{r_max} set to 0.25 for different sets of α_1 and α_2 parameters.

All soils in this study had at least 60 cm depth of fine earth soil material, with most sites classifying to the Pallic soil order in the New Zealand Soil Classification (Hewitt, 2010), correlating in Soil Taxonomy to Haplusteps and Humustepts great groups. Fourteen sites had younger soils that classified to the Recent soil order (Hewitt, 2010), correlating to Haplusteps and Ustifluvent great groups. Variation of particle size occurs in these soils due to factors such as the distance from the river source (coarser textures near source), nature of deposition (loess soils often have a higher silt content), and degree of weathering, with older soils having more compact subsoils and sometimes greater clay content due to argillisation processes.

Soil was sampled in 10 cm increments to 60 cm depth. At each increment two soil cores were collected, a large core of 589 cm^3 (10 cm diameter by 7.5 cm depth) used for unsaturated hydraulic conductivity measurements, and a small core of 59 cm^3 (5 cm diameter by 3 cm depth) used for water retention measurements. At the same depth increments and immediately beside the soil cores, a bulk sample was collected for particle size and chemistry measurement. To ensure consistent soil moisture conditions at all sites water was infiltrated two days prior to sampling.

For each core that was sampled, a column of soil was created by sitting a core liner on the soil surface and carefully carving down around the core with a sharp knife, leaving the core sitting on a pedestal a few mm wider than itself. Soil core liners were slowly and carefully pushed down into the soil, while trimming the sides of the pedestal. This process prevented any disturbance or damage to the soil structure, ensuring that the properties of the cores that were analysed were the same as the soil in situ at the sampling site.

All cores were immediately wrapped in plastic film, packed into crates with foam lining and stored at 4 °C until laboratory measurement could occur.

3.1.2. Soil physical measurements

Soil core preparation, bulk density, particle density, water retention and unsaturated hydraulic conductivity were measured at the Manaaki Whenua national soil physics laboratory, following the standard methods used in New Zealand (Gradwell, 1972; Gradwell and Birrell, 1979; Claydon, 1989). These methods are summarised below.

Particle density was determined for each depth increment as described in Gradwell and Birrell (1979). Particle density values ranged from 2.52 g cm^3 to 2.75 g cm^3 (standard deviation of 0.05 g cm^3), with topsoil values slightly lower than that found in subsoil.

Bulk density was measured for both large and small cores, following the water release and unsaturated conductivity measurements. Dry soil weight was measured after oven drying at 105 °C for 24 h. Despite the differences in sample volume, the correlation between large cores and small core bulk density measurements shows a coefficient of determination of 0.842 with a deviation from the 1:1 line lower than 0.5% (slope 0.995).

The particle size distribution of the soil fine earth fraction (<2.00 mm) was measured by wet sieving and the pipette method, as described in Claydon (1989). Samples were pre-treated to remove organic matter and calcium carbonate if necessary, and then dispersed by ultrasonic vibration and a chemical dispersant agent. The coarser fraction (>0.063 mm) was wet sieved, dried and shaken through a stack of sieves between sizes 2.00 mm and 0.063 mm. The remaining soil <0.063 mm was suspended in a column and, after initial shaking, pipette samples are drawn at various times from a set depth to determine the concentration of particles, following Stokes' equation.

The soils collected had *Loamy silt, Sandy loam, Silt loam and Silty clay* texture classes according to New Zealand soil classification (Milne et al., 1995). Fig. 4 presents the textural triangle corresponding to the collected samples.

Water retention values were measured at 0.4, 0.7, 1, 5, 10, 20, 40, 100 and 1500 kPa for the small cores. Measurements <10 kPa suction were on high flow ceramic plates, with suction applied by a hanging water column. Measurements above 10 kPa suction were made using pressure chambers (Gradwell and Birrell, 1979). Additional measurements taken on large cores at 5 and 10 kPa showed high correlation with values obtained for the small cores with coefficients of determinations of 0.883 (slope 1.007) and 0.892 (slope 1.001), respectively.

For representativeness and to better capture the soil structure, the large core bulk density data were used to convert gravimetric soil water content into the corresponding volumetric values. Saturated water content, θ_s, was obtained from the soil porosity, ϕ, derived for the large cores using the soil particle density and bulk density. The θ_s is related to ϕ by a multiplying factor representing the ratio of measured saturated water content to calculated porosity out of the measured bulk density, $\theta_s = \varepsilon\phi$, where ε is set to 0.95, slightly increasing the goodness of the fit of the hydraulic parameters. For a limited number of samples with water retention value at 0.4 kPa higher than porosity, the small core bulk density was used instead.

To measure unsaturated hydraulic conductivity the large cores were trimmed, saturated and then equilibrated to 0.1, 0.4, 0.7 and 1 kPa suction with a Buchner funnel apparatus, as described in Cook et al. (1993). Unsaturated hydraulic conductivity was then measured using disc permeameters set to equivalent suctions for each measurement (Cook et al., 1993).

3.2. Kosugi hydraulic model

The $\theta(\psi)$ is often expressed as a close-form unimodal function representing the relationship between θ and ψ (e.g. Brooks and Corey, 1964; Clapp and Hornberger, 1978; van Genuchten, 1980). Among these functions, the one proposed by Kosugi, (1996) has the advantage of having parameters with a direct physical meaning in relation to the soil pore-size distribution (e.g. Hayashi et al., 2009; Pollacco et al., 2013, 2017). The unimodal lognormal distribution of pores in the soil matrix leads to the Kosugi model for the $\theta(\psi)$:

$$\theta = \frac{1}{2}(\theta_s - \theta_r)\,\mathrm{erfc}\left(\frac{\ln\psi - \ln\psi_m}{\sigma\sqrt{2}}\right) + \theta_r \tag{24}$$

where θ_r is the residual volumetric water content, erfc is the complementary error function, while ψ_m [L] and σ [-] are the shape parameters of the water retention curve. In a physical sense $\ln\psi_m$ refers to the median of the lognormal distribution of the matric potential, which corresponds to the logarithmic median of the effective soil pore radius through the Young-Laplace capillary equation, $\ln r_m$, and σ is the standard deviation of the log-transformed soil pore radius. The unsaturated hydraulic conductivity function for the Kosugi model can be written as:

$$K(S_e) = K_s\sqrt{S_e}\,\mathrm{erfc}\left(\frac{1}{2}\mathrm{erfc}^{-1}\left(2S_e + \frac{\sigma}{\sqrt{2}}\right)\right)^2 \tag{25}$$

where K_s [L T^{-1}] is the saturated hydraulic conductivity and S_e [−] refers to the effective saturation.

$$S_e = \frac{\theta - \theta_r}{\theta_s - \theta_r} \tag{26}$$

Values derived from the fit of the experimental data to the Kosugi hydraulic model for the individual soils are considered as observed data for the fitting of the PSD models.

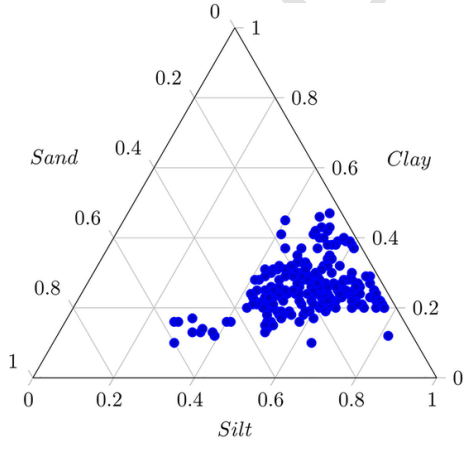

Fig. 4. Textural triangle for the soils of the studied area.

3.3. Objective function and goodness of fit

The fitting process used to estimate the parameters used a robust global optimizer BlackBoxOptim (https://github.com/robertfeldt/BlackBoxOptim.jl) written in the Julia language (Bezanson et al., 2017). This procedure used an objective function and goodness-of-fit defined in the following sections.

3.3.1. Inverting procedure to derive $\theta(\psi)$ from experimental data

The minimization process between the observed and the fitted values used an objective function, OF_{kg} (see below), that includes information from both the water retention $\theta(\psi)$ and hydraulic conductivity $K(\psi)$ data, in order to avoid problems of non-uniqueness. The ln transformation in the second term of the OF_{kg} puts relatively more weight on the lower values of $K(\theta)$ to minimize the bias toward high conductivity, and also takes into account the larger uncertainties in measuring $K(\theta)$ as it increases (Pollacco et al., 2013). The feasible range of parameters used for the fit is set according to Fernández-Gálvez et al. (2019). The OF_{kg} is computed as follows:

$$OF_{kg} = \frac{\sum_{i=1}^{l}\left(\theta(\psi)_{obs_i} - \theta(\psi)_{kg_i}\right)^2}{\sum_{i=1}^{l}\left(\theta(\psi)_{obs_i} - \overline{\theta(\psi)_{obs}}\right)^2} + \frac{\sum_{i=1}^{k}\left(\ln\left(1 + K(\theta)_{obs_i}\right) - \ln\left(1 + K(\theta)_{kg_i}\right)\right)^2}{\sum_{i=1}^{k}\left(\ln\left(1 + K(\theta)_{obs_i}\right) - \overline{\ln\left(1 + K(\theta)_{obs}\right)}\right)^2} \tag{27}$$

where l and k refer to the total number of experimentally measured data for the water retention and the unsaturated hydraulic conductivity curves respectively. $\theta(\psi)_{obs_i}$ and $K(\theta)_{obs_i}$ correspond to the experimental values measured for the $\theta(\psi)$ and hydraulic conductivity function, respectively, and $\theta(\psi)_{kg_i}$ and $K(\theta)_{kg_i}$ correspond to fitted values of the Kosugi model. The fitted soil hydraulic parameters are therefore ψ_m, σ, θ_r and K_s; θ_s is obtained experimentally from bulk density.

The goodness of fit of the measured water retention data to the $\theta(\psi)$ using the Kosugi model was assessed using the Nash-Sutcliffe efficiency coefficient, $NSE_{\theta(\psi)}$, as follows:

$$NSE_{\theta(\psi)} = 1 - \frac{\sum_{i=1}^{l}\left(\theta(\psi)_{obs_i} - \theta(\psi)_{kg_i}\right)^2}{\sum_{i=1}^{l}\left(\theta(\psi)_{obs_i} - \overline{\theta(\psi)_{obs}}\right)^2} \tag{28}$$

where l corresponds to the total number of data points experimentally measured in the $\theta(\psi)$, $\theta(\psi)_{obs_i}$ corresponds to the experimental val-

ues measured to derive the $\theta(\psi)$, and $\theta(\psi)_{kg_i}$ corresponds to the values derived from the fitted Kosugi model. A similar approach is used to quantify the goodness of the fit for $K(\theta)$ using the corresponding $NSE_{K(\theta)}$ with the hydraulic conductivity values.

3.3.2. Inverting procedure to derive $\psi(\theta)$ from PSD

The minimization process between the "observed" $\theta(\psi)_{kg_i}$ derived from the fitted Kosugi model and the fitted PSD models described in Table 2 used the following objective function, OF_{psd}:

$$OF_{psd} = \sum_{i=1}^{m}\left(\theta(\psi)_{psd_i} - \theta(\psi)_{kg_i}\right)^2 \quad (29)$$

where m refers to the total number of data points of the PSD data. The capability of the different particle size distribution models to predict the experimentally determined $\theta(\psi)$ is also evaluated using the Nash–Sutcliffe efficiency coefficient, $NSE_{\theta(\psi)_{psd}}$, defined as follows:

$$NSE_{\theta(\psi)_{psd}} = 1 - \frac{\sum_{i=1}^{m}\left(\theta(\psi)_{kg_i} - \theta(R)_{psd_i}\right)^2}{\sum_{i=1}^{m}\left(\theta(\psi)_{kg_i} - \overline{\theta(\psi)_{kg}}\right)^2} \quad (30)$$

where m corresponds to the total number of data points in the $\theta(\psi)$, $\theta(\psi)_{kg_i}$ corresponds to the laboratory values fitted to the $\theta(\psi)$ using the Kosugi model, and $\theta(R)_{psd_i}$ corresponds to the estimated value of the $\theta(\psi)$ from the corresponding particle size distribution model described in Table 2.

4. Results and discussion

4.1. Experimental data and fitting of the laboratory $\theta(\psi)$

Table 1 summarises the statistics of the prominent measured soil physical properties (ρ_s, ρ_b and θ_s) and fitted Kosugi hydraulic parameters (K_s, Ψ_m, σ, and θ_r) derived by minimizing OF_{kg} (Eq. (27)) using laboratory measurements. The highest variability occurs for $\ln K_s$, indicating the wide range of permeability of the studied soils. The variability of $\ln \psi_m$ and σ, close to 20%, illustrates the range of the hydraulic properties of the studied soils. The goodness of fit of the observed data to the Kosugi hydraulic model (Eq. (28)) is equally good for $\theta(\psi)$ (Eq. (24)) and $K(\psi)$ (Eq. (25)), with mean NSE values of 0.92 (SD 0.09) and 0.94 (SD 0.10), respectively.

4.2. Derive θ_r from PSD

Fig. 5 (left) shows the relationship between the estimated θ_r values derived from the fit of the experimental data to the Kosugi hydraulic model (observed, $\theta_{r\ kg}$) for the individual soils as a function of the clay content and the estimated θ_r values predicted with Eq. (23) from clay (predicted, $\theta_{r\ psd}$). The NSE coefficient between the observed and predicted values is 0.60, with optimal α_1 and α_2 parameters equal to 16.02 and 2.01, respectively for the studied soils. Fig. 5 (right) shows θ_r observed and predicted values closely align to the 1:1 line. Predicted values from Eq. (23) slightly overestimate θ_r compared to the fitted values, with a slope equal to 0.98.

4.3. Intergranular mixing function from PSD

The fitting parameters ξ_1 and ξ_2 describing the bell shape of $R_i^{-\xi(R_i)}$ (Fig. 2) when ξ is described by Eq. (21) were found to be highly correlated. ξ_1 is less sensitive than ξ_2 to both the amplitude and the location of the maxima in the weighting applied to the $\sum PSD$. Therefore, ξ_1 was kept constant at an optimal value for all soils, while ξ_2 was derived for every soil sample from Eq. (22) (Table 2, step 4). For the soils studied, ξ_2 was highly correlated with $\sum PSD = 0.003$ mm particle radius ($p = 2$ in Eq. (22), corresponding to particle sizes up to the very fine silt fraction). The NSE coefficient between ξ_2 values obtained for individual soils (Table 2, step 3) and predicted values of ξ_2 derived from Eq. (22) is 0.49, with optimal values of $\beta_1 = 0.09$ and $\beta_2 = 0.95$, and an associated $\xi_1 = 9.04$ (Table 2, step 4). These three parameters are the optimised IMP model parameters obtained for the soils studied.

Table 1
Soil physical properties and fitted Kosugi hydraulic parameters to laboratory measurements. Mean, standard deviation (SD), coefficient of variation (CV), maximum and minimum values for the 259 soils studied.

	ρ_s [g cm $^{-3}$]	ρ_b [g cm $^{-3}$]	θ_s [cm ^{3} cm $^{-3}$]	$\ln K_s$ [cm h $^{-1}$]	$\ln \psi_m$ [cm]	σ[–]	θ_r [cm ^{3} cm $^{-3}$]
Mean	2.66	1.44	0.44	2.42	5.98	2.56	0.15
SD	0.05	0.16	0.06	1.81	1.04	0.50	0.06
CV (%)	1.90	10.93	12.81	74.63	17.35	19.48	37.33
max	2.75	1.81	0.61	3.77	8.70	4.30	0.25
min	2.52	1.00	0.33	−3.52	4.38	1.40	0.00

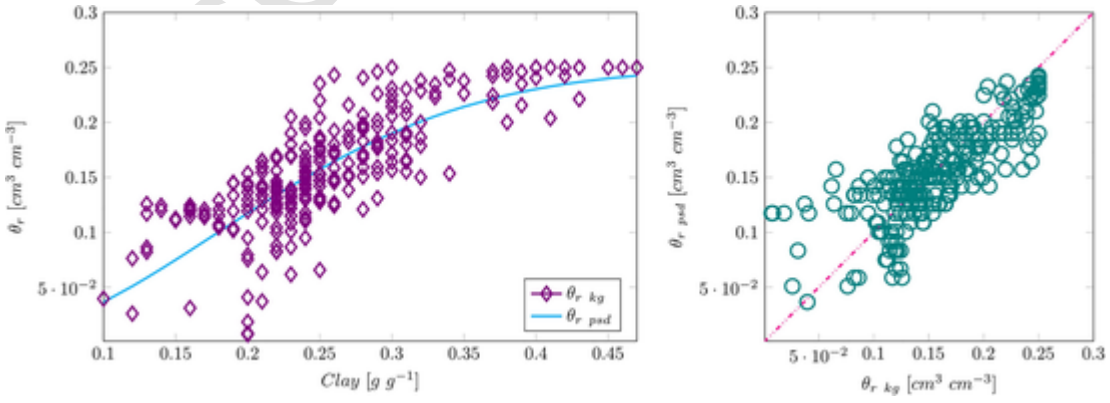

Fig. 5. Fitted (observed) values of θ_r from experimental data and predicted with Eq. (23) from clay for the studied soils (left), together with the comparison between the fitted and the predicted values of θ_r (right).

Table 2
Model development steps to derive $\theta(\psi)$ from PSD and associated $NSE_{\theta(\psi)_{psd}}$ (mean and standard deviation).

	$NSE_{\theta(\psi)_{psd}}$	
	Mean	SD
Chang et al., 2019	0.53	0.32
$\begin{cases} \theta_1 = \theta_s Clay^{\eta} & \text{with } \eta \text{ optimised} \\ \theta_i = \theta_1 + \theta_s \sum_{j=2}^{i} \left(w_i - (Clay^{\eta} - Clay) \frac{w_i}{\sum_{j=2}^{m} w_j} \right) & \text{for } i > 1 \end{cases}$		
$\psi_i = \frac{Y}{0.3 R_i}$		
Model development steps	Mean	SD
1. Normalised Young–Laplace capillary equation for Ψ due to limited range of the smallest PSD and normalised θ from PSD corrected for non-sphericity of soil particles	0.48 ($\lambda = 1$) 0.85 ($\lambda = 2$)	0.30 ($\lambda = 1$) 0.22 ($\lambda = 2$)
$\theta_i = \theta_s \frac{\sum_{j=1}^{i} w_j R_j^{-\xi}}{\sum_{j=1}^{m} w_j R_j^{-\xi}}$; ξ optimised		
$\psi_i = \psi_{Max} \cdot \left(\frac{\frac{1}{R_i} - \frac{1}{R_{Max}}}{\frac{1}{R_{Min}} - \frac{1}{R_{Max}}} \right)^{\lambda}$; ψ_{Max} = constant and λ = 1 or 2		
2. Residual pore volume for θ due to limited range of the smallest PSD	0.85	0.17
$\theta_i = (\theta_s - \theta_{r\ psd}) \frac{\sum_{j=1}^{i} w_j R_j^{-\xi}}{\sum_{j=1}^{m} w_j R_j^{-\xi}} + \theta_{r\ psd}$; ξ optimised		
$\theta_{r\ psd} = \theta_{r\_max} \left(1 - \exp\left(-\alpha_1 \cdot Clay^{\alpha_2}\right)\right)$		
$\psi_i = \psi_{Max} \cdot \left(\frac{\frac{1}{R_i} - \frac{1}{R_{Max}}}{\frac{1}{R_{Min}} - \frac{1}{R_{Max}}} \right)^{\lambda}$; ψ_{Max} (constant and λ = 2)		
3. Intergranular mixing of soil particles depending on their size	0.88	0.16
$\theta_i = (\theta_s - \theta_{r\ psd}) \frac{\sum_{j=1}^{i} w_j R_j^{-\xi}}{\sum_{j=1}^{m} w_j R_j^{-\xi}} + \theta_{r\ psd}$		
$\xi_1(R_i) = \xi_1 \exp\left(-R_i^{-\xi_2}\right)$; ξ_1 and ξ_2 optimised		
$\theta_{r\ psd} = \theta_{r\_max} \left(1 - \exp\left(-\alpha_1 \cdot Clay^{\alpha_2}\right)\right)$		
$\psi_i = \psi_{Max} \cdot \left(\frac{\frac{1}{R_i} - \frac{1}{R_{Max}}}{\frac{1}{R_{Min}} - \frac{1}{R_{Max}}} \right)^{\lambda}$; ψ_{Max} (constant and λ = 2)		
4. Intergranular mixing of soil particles depending on their size as a function of PSD	0.92	0.08
$\theta_i = (\theta_s - \theta_{r\ psd}) \frac{\sum_{j=1}^{i} w_j R_j^{-\xi}}{\sum_{j=1}^{m} w_j R_j^{-\xi}} + \theta_{r\ psd}$		
$\xi(R_i) = \xi_1 \exp\left(-R_i^{-\xi_2}\right)$; ξ_1 optimised		
$\xi_1 = \beta_1 \exp\left(\beta_2 \sum_{i=1}^{p} w_i\right)$; β_1 and β_2 optimised for p = 2		
$\theta_{r\ psd} = \theta_{r\_max} \left(1 - \exp\left(-\alpha_1 \cdot Clay^{\alpha_2}\right)\right)$		
$\psi_i = \psi_{Max} \cdot \left(\frac{\frac{1}{R_i} - \frac{1}{R_{Max}}}{\frac{1}{R_{Min}} - \frac{1}{R_{Max}}} \right)^{\lambda}$; ψ_{Max} = constant and λ = 2		

For illustration purposes, Fig. 6 (left) shows $\sum PSD$ for two soils with contrasting texture (fine and coarse texture soils). Fig. 6 (right) relates $\sum PSD$ at 0.003 mm particle radius (marked with a vertical dashed line in Fig. 6 left) to ξ_2 (Eq. (22)). As expected, the slope of $\sum PSD$ up to the fine silt fraction increases with the amount of clay and fine silt. This results in a decrease in the general slope of $\sum PSD$ when passing from fine texture to coarse texture soils, which is directly related to the shape of the $\theta(\psi)$. For sandy soil the $\theta(\psi)$ is steeper than for a clay soil. Computed values of ξ_2 for the individual soils as a function of the $\sum PSD$ up to the 0.003 mm particle radius are plotted together with the fitting corresponding to Eq. (22) (Fig. 6, right).

4.4. Physical processes to derive $\theta(\psi)$ from PSD

For each progressive step of the model $NSE_{\theta(\psi)_{psd}}$ steadily increases and SD decreases, (Table 2), showing that taking into account further processes improves model performance. The processes taken into account at each model development step are outlined below:

Step 1: Normalised Young–Laplace capillary equation for Ψ due to limited range of the smallest PSD and normalised θ from PSD corrected for non-sphericity of soil particles

The first step derives the $\theta(\psi)$ from PSD data by calculating θ from a normalised expression of the $\sum PSD$ scaled by θ_s and corrected for the non-sphericity of the soil particles (Eq. (18)) through ξ optimised for all soils. The simplification of the soil pore system to perfectly spherical pores ($\xi = 0$) reduces the performance of derivation of $\theta(\psi)$ from PSD since soil pores are not perfectly spherical. Ψ is computed from R using the normalised expression of the Young–Laplace capillary equation (Eq. (20)), resulting in a significant improvement when increasing λ from 1 to 2 to account for the larger suction corresponding to the small pores. This correction considers the limitation in describing the smallest pore sizes from the smallest particle size fraction (clay) when assuming similarity between $\sum PSD$ and $\theta(\psi)$. The corresponding optimal values are $\xi = 0.79$ for $\lambda = 1$ ($NSE_{\theta(\psi)_{psd}} = 0.48$) and $\xi = 0.08$ for $\lambda = 2$ ($NSE_{\theta(\psi)_{psd}} = 0.85$). The improvement in the model when $\lambda = 2$ with $\xi = 0.08$ suggests that pores are almost spherical. These results already outperform alternative attempts presented in the literature (e.g. Mohammadi and Vanclooster, 2011; Meskini-Vishkaee et al., 2014; Chang et al., 2019).

Step 2: Residual pore volume for θ due to limited range of the smallest PSD

The soil porous media is able to retain water that is strongly bound to solid particles or in very small pores that remain in the soil at a suction higher than 1500 kPa. Therefore, introducing a residual pore volume considered as a residual soil water content slightly increases the model performance (SD reduced from 0.22 to 0.17). The improvement by using a residual pore volume, considered as a residual soil water content and related to the clay fraction by Eq. (23), is not reflected in the mean value of the $NSE_{\theta(\psi)_{psd}}$ because it is more sensitive to errors in large pores than in small pores.

Step 3: Intergranular mixing of soil particles depending on their size

The mixing of soil particles is affected by the particle size. This is considered in Eq. (21), where optimizing ξ_1 and ξ_2 for all soils improves the prediction of the $\theta(\psi)$ from PSD. This confirms that soil particle arrangements in the soil can have neighbouring particles of different sizes, which results in variations in pore radius and pore shape of the corresponding pore fraction. In fact, the particle radius represents an effective mean radius for each of the particle fractions. The optimal values for ξ_1 and ξ_2 are 11.07 and 0.12, respectively. The weighting applied to the $\sum PSD$ to translate it into the $\theta(\psi)$ has the form of a bell shape with larger corrections applied in the middle range of the particle sizes, because statistically higher mixing occurs for effective mid-sized particles.

Step 4: Intergranular mixing of soil particles depending on their size as a function of PSD

It was found that ξ_1 and ξ_2 in Eq. (21) are highly correlated, with ξ_2 showing higher sensitivity to $R_i^{-\xi(R_i)}$ than ξ_1. Additionally, ξ_2 is correlated to the amount of particles below 0.003 mm radius, allowing ξ_2 to be derived from PSD using Eq. (22). This improves the estimates of $\theta(\psi)$ from PSD using only 3 parameters: β_1, β_2 (to derive ξ_2), and ξ_1. Therefore, the IMP model can accurately predict $\theta(\psi)$ from experimental measurements of PSD and θ_s.

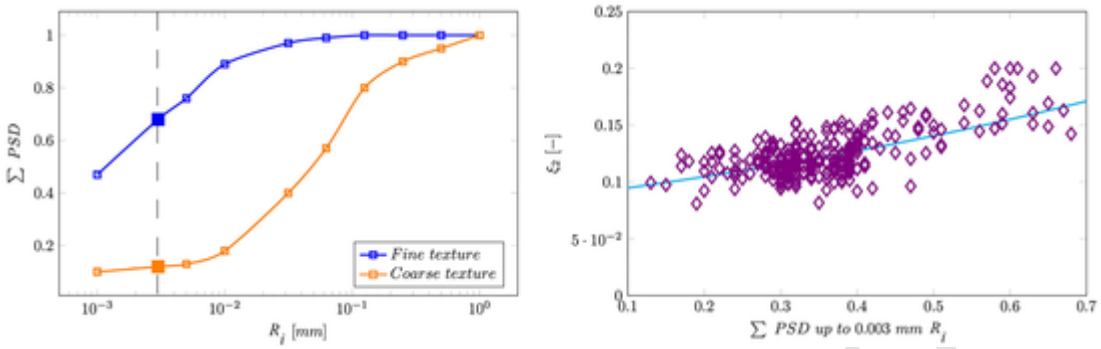

Fig. 6. (Left) $\sum PSD$ as a function of R for selected soil samples with contrasting soil texture. $\sum PSD$ at 0.003 mm particle radius is highlighted (vertical dashed line) as it is directly related to ξ_2. (Right) Values of ξ_2 obtained for individual soils as a function of $\sum PSD$ up to 0.003 mm particle radius (violet) and relationship described by Eq. (22) (cyan). (For interpretation of the references to colour in this figure legend, the reader is referred to the web version of this article.)

4.5. Model performance to derive $\theta(\psi)$ from PSD

The proposed IMP model (Table 2, step 4) is compared to the Chang et al. (2019) model. The residual pore fraction used in Chang et al. (2019) is related to the clay fraction by a power function for which they obtained a fitting value of η equal to 0.52 for a data set including clay to sandy soil textures. Optimising this fitting parameter for our studied soils gave $\eta = 0.55$, which slightly increased the model performance. Nevertheless, the Chang et al (2019) model gave considerably less robust agreement between the observed and predicted $\theta(\psi)$ ($NSE_{\theta(\psi)_{psd}} = 0.53$ and SD = 0.32) compared to our novel model with optimized β_1, β_2 and ξ_1 ($NSE_{\theta(\psi)_{psd}} = 0.92$ and SD = 0.08). Chang et al. (2019) pointed out the limitations of their model for silty soils, and therefore the significant amount of silt in the soils in this study will have contributed to the poorer agreement of their model. Increasing silt content contributes to more intergranular mixing of soil particles, which results in wider variations in corresponding pore shapes and sizes. Therefore, a stronger correction needs to be applied at this particle size range to derive $\theta(\psi)$ from PSD for silty soils.

The IMP model performs very well for all soil groups (Table 3), with marginally worse performance for *sandy loam* ($NSE_{\theta(\psi)_{psd}} = 0.87$), which may be due to the small sample size. The IMP model was remarkably successful making predictions for *loamy* and *silty* soils, which are considered to be the most difficult soils to be modelled (Chang et al., 2019; Fernández-Gálvez et al., 2019; Haverkamp and Parlange, 1986; Mohammadi and Vanclooster, 2011; Nimmo et al., 2007; Zhuang et al., 2001).

Although we were able to successfully model $\theta(\psi)$, we were not able to directly compare the optimal hydraulic parameters from the Kosugi model (or any other hydraulic model) derived from the $\theta(\psi)$ derived from laboratory measurements with the hydraulic parameters derived from the IMP model. This limitation arises because equally good combinations of hydraulic parameters could be derived, which are "sets of truly linked parameters" (Pollacco et al., 2008a, 2008b; Pollacco and Angulo-Jaramillo, 2009; Fernández-Gálvez et al., 2019). This is because the IMP model derives $\theta(\psi)$ but no estimate is provided for $K(\theta)$ to act as a constraint for the resolution of non-uniqueness. This issue will be the subject of further investigation.

Examples for each of the soil texture groups (Fig. 7) show the IMP model predicts similar $\theta(\psi)$ to those derived from laboratory measurements. In general, the deviations between observed and predicted $\theta(\psi)$ are random and small (Fig. 7d).

The bell shape of the weighting function (Fig. 7c) accounts for the intergranular mixing of particles. The location of the mode depends on soil texture and shifts within the silt particle size range. As indicated in Section 2.3.1, the displacement of the mode is related to the degree of intergranular mixing of the soil particles. Increasing smaller particles in a "polydisperse soil" results in higher intergranular mixing and therefore, the correction spreads to a wider range of larger particles (the width of the bell increases). As expected, for *Sandy loam* soils the mode shifts towards the smaller silt sizes, while for *silty clay* soils the mode shifts towards the larger silt sizes.

Table 3
$NSE_{\theta(\psi)_{psd}}$ coefficients for the soil texture groups for all studied soils.

Soil texture	Number of soils	$NSE_{\theta(\psi)_{psd}}$	
		Mean	SD
Loamy silt	12	0.93	0.09
Sandy loam	9	0.87	0.06
Silt loam	212	0.93	0.08
Silty clay	26	0.94	0.05
Total	259	0.92	0.08

5. Conclusions

This paper develops a novel, physically based, intergranular mixing PSD model, (IMP), which derives $\theta(\psi)$ from traditional PSD data. The model exploits the relationship between particle size and pore size distributions and the intergranular arrangement of the soil particles. The IMP model successfully predicts $\theta(\psi)$ for fine texture soils, which are the most challenging soil textures to be modelled. Reliable estimates of $\theta(\psi)$ can be obtained in a cost-effective way from PSD and θ_s using only three general fitting parameters (mean Nash–Sutcliffe efficiency coefficient 0.92 for 259 soils) without requiring an assumption of soil particle packing type.

The IMP model can accurately predict $\theta(\psi)$ for fine texture soils because a) it implements an intergranular mixing function that accounts for soil pores not all being perfectly spherical and takes into consideration the intergranular rearrangement (mixing) of the particles, which allows neighbouring particles to have different sizes resulting in variations in pore radius and pore shape of the corresponding pore fraction; b) it overcomes the absence of PSD data below the clay fraction by developing a normalised form of the Young–Laplace capillary equation; and c) the residual pore volume accounting for water strongly bound to the solid particles or in very small pores is incorporated as a function of the clay fraction. This leads to the conclusion that to compute $\theta(\psi)$ from PSD the proposed model only requires ρ_b to calculate θ_s and three general fitting parameters β_1, β_2 to compute ξ_2, and ξ_1.

Despite of the excellent agreement between the water retention curve derived from laboratory measurements and from the IMP model, it was not possible to compare the derived hydraulic parameters due to the problem of non-uniqueness. This issue needs be the subject to further investigation by the hydrological community. Further work is also recommended to test and calibrate the IMP model on a wider range

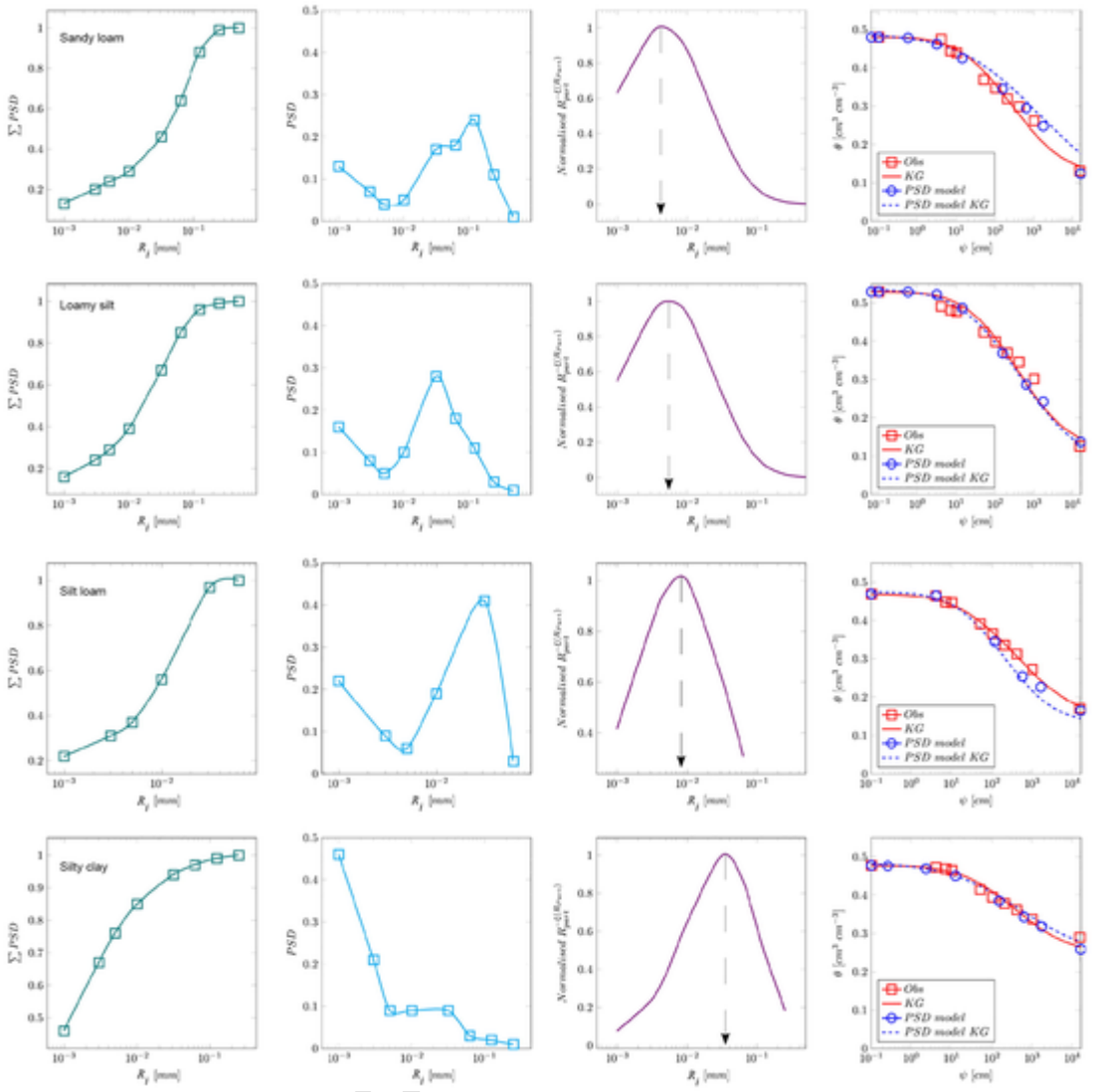

Fig. 7. Examples of model performance to derive $\theta(\psi)$ from PSD for each of the texture groups shown in Table 3: a) $\sum PSD$, b) PSD, c) normalised weighting function modulating $\sum PSD$ to account for intergranular mixing as a function of particle radius (the arrow indicates the location of the mode), and d) fit of $\theta(\psi)$ derived from laboratory (experimental values and optimal fit to the Kosugi model in red) and from the IMP model (derived values and optimal fit to the Kosugi model in blue). (For interpretation of the references to colour in this figure legend, the reader is referred to the web version of this article.)

of soils with different parent material and mineralogy.

Declaration of Competing Interest

The authors declare that they have no known competing financial interests or personal relationships that could have appeared to influence the work reported in this paper.

Acknowledgements

Funding provided by the New Zealand Ministry for Business, Innovation and Employment under the MBIE S-map Next Generation research programme and the MBIE Winning against wildings. John Dando for the laboratory physical determinations, Veronica Penny for collecting soil cores and samples, Laurent Lassabatere and Rafael Angulo-Jaramillo for helpful discussion on soil pore medium, and Stephen McNeill and Leah Kearns for reviewing and improving the manuscript.

References

Allbrook, R.F., 1993. Shrinkage of some New Zealand soils and its implications for soil physics. Aust. J. Soil Res. 31 (2), 111–118. doi:10.1071/SR9930111.

Arya, L.M., Bowman, D.C., Thapa, B.B., Cassel, D.K., 2008. Scaling soil water characteristics of golf course and athletic field sands from particle-size distribution. Soil Sci. Soc. Am. J. 72, 25. doi:10.2136/sssaj2006.0232.

Arya, L.M., Paris, J.F., 1981. A physicoempirical model to predict the soil moisture characteristic from particle-size distribution and bulk density data. Soil Sci. Soc. Am. J. 45, 1023–1030. doi:10.2136/sssaj1981.03615995004500060004x.

Balland, V., Pollacco, J.A.P., 2008. Modeling soil hydraulic properties for a wide range of soil conditions. Ecol. Model. 219, 300–316.

Bezanson, J., Edelman, A., Karpinski, S., Shah, V.B., 2017. Julia: a fresh approach to numerical computing. SIAM Rev. 59, 65–98. doi:10.1137/141000671.

Brooks, R.H., Corey, A.T., 1964. Hydraulic properties of porous media. Hydrology Papers 3 27, 3.

Bruce, J.G. (Ed.), 1984. Soil Groups of New Zealand. Part 7, Yellow-grey earths. New Zealand Society of Soil Science, Lower Hutt, New Zealand, p. 123.

Chang, C., Cheng, D., Qiao, X., 2019. Improving estimation of pore size distribution to predict the soil water retention curve from its particle size distribution. Geoderma 340, 206–212. doi:10.1016/j.geoderma.2019.01.011.

Clapp, R.B., Hornberger, G.M., 1978. Empirical equations for some soil hydraulic properties. Water Resour. Res. 14, 601–604. doi:10.1029/WR014i004p00601.

Claydon, J.J., 1989. Determination of particle size in fine grained soils – pipette method. DSIR Division of Land and Soil Sciences Technical Record LH5.

Cook, F.J., Lilley, G.P., Nunns, R.A., 1993. Unsaturated hydraulic conductivity and sorptivity: laboratory measurement. In: Carter, M.R. (Ed.), Soil Sampling and Methods of Analysis. Lewis Publishers, Boca Raton, pp. 615–624.

Fernández-Gálvez, J., Barahona, E., 2005. Changes in soil water retention due to soil kneading. Agric. Water Manag. 76, 53–61. doi:10.1016/j.agwat.2005.01.004.

Fernández-Gálvez, J., Pollacco, J.A.P., Lassabatere, L., Angulo-Jaramillo, R., Carrick, S., 2019. A general Beerkan Estimation of Soil Transfer parameters method predicting hydraulic parameters of any unimodal water retention and hydraulic conductivity curves: application to the Kosugi soil hydraulic model without using particle size distribution data. Adv. Water Resour. 129, 118–130. doi:10.1016/j.advwatres.2019.05.005.

Gradwell, M.W., 1972. Methods for physical analysis of soils New Zealand Soil Bureau Scientific Report 10C, p. 59.

Gradwell, M.W., Birrell, K.S., 1979. Methods for physical analysis of soils New Zealand Soil Bureau Scientific Report 10C, p. 62.

Haverkamp, R., Parlange, J., 1986. Predicting the water-retention curve from particle-size distribution: 1. sandy soils without organic matter. Soil Sci. 142, 325–339.

Hayashi, Y., Kosugi, K., Mizuyama, T., 2009. Soil water retention curves characterization of a natural forested hillslope using a scaling technique based on a lognormal pore-size distribution. Soil Sci. Soc. Am. J. 73, 55–64.

Hewitt, A.E., 2010. New Zealand Soil Classification. third ed. Landcare Research, Lincoln, New Zealand, p. 136.

Klute, A., 1986. Methods of Soil Analysis. Part 1 Physical and Mineralogical Properties. American Society of Agronomy, Madison, Wisconsin.

Kosugi, K., 1996. Lognormal distribution model for unsaturated soil hydraulic properties. Water Resour. Res. 32, 2697–2703. doi:10.1029/96WR01776.

Landcare Research New Zealand Ltd, 2011. S-map: The digital soil map for New Zealand. https://doi.org/10.7931/l1wc7.

Lee, T.-K., Ro, H.-M., 2014. Estimating soil water retention function from its particle-size distribution. Geosci. J. 18, 219–230. doi:10.1007/s12303-014-0017-7.

McNeill, S.J., Lilburne, L., Carrick, S., Webb, T., Cuthill, T., 2018. Pedotransfer functions for the soil water characteristics of New Zealand soils using S-map information. Geoderma 326, 96–110. doi:10.1016/j.geoderma.2018.04.011.

Meskini-Vishkaee, F., Mohammadi, M.H., Vanclooster, M., 2014. Predicting the soil moisture retention curve, from soil particle size distribution and bulk density data using a packing density scaling factor. Hydrol. Earth Syst. Sci. 18, 4053–4063. doi:10.5194/hess-18-4053-2014.

Milne, J.D.G., Clayden, B., Singleton, P.L., Wilson, A.D., 1995. Soil Description Handbook. Manaaki Whenua Press. ed. Lincoln, New Zealand.

Mohammadi, M.H., Meskini-Vishkaee, F., 2013. Predicting soil moisture characteristic curves from continuous particle-size distribution data. Pedosphere 23, 70–80.

Mohammadi, M.H., Vanclooster, M., 2011. Predicting the soil moisture characteristic curve from particle size distribution with a simple conceptual model. Vadose Zone J. 10, 594. doi:10.2136/vzj2010.0080.

Nasta, P., Romano, N., Assouline, S., Vrugt, J.A., Hopmans, J.W., 2013. Prediction of spatially variable unsaturated hydraulic conductivity using scaled particle-size distribution functions: simultaneous scaling. Water Resour. Res. 49, 4219–4229. doi:10.1002/wrcr.20255.

Nimmo, J.R., Herkelrath, W.N., Luna, A.M.L., 2007. Physically Based Estimation of Soil Water Retention from Textural Data: General Framework, New Models, and Streamlined Existing ModelsAll rights reserved. No part of this periodical may be reproduced or transmitted in any form or by any means, electronic or mechanical, including photocopying, recording, or any information storage and retrieval system, without permission in writing from the publisher. Vadose Zone J. 6, 766–773. doi:10.2136/vzj2007.0019.

Pollacco, J.A.P., 2008. A generally applicable pedotransfer function that estimates field capacity and permanent wilting point from soil texture and bulk density. Can. J. Soil Sci. 88, 761–774.

Pollacco, J.A.P., Angulo-Jaramillo, R., 2009. A Linking Test that investigates the feasibility of inverse modelling: application to a simple rainfall interception model for Mt. Gambier, southeast South Australia. Hydrol. Process. 23, 2023–2032.

Pollacco, J.A.P., Braud, I., Angulo-Jaramillo, R., Saugier, B., 2008. A Linking Test that establishes if groundwater recharge can be determined by optimising vegetation parameters against soil moisture. Ann. Forest Sci. 65.

Pollacco, J.A.P., Nasta, P., Ugalde, J.M.S., Angulo-Jaramillo, R., Lassabatere, L., Mohanty, B.P., Romano, N., 2013. Reduction of feasible parameter space of the inverted soil hydraulic parameters sets for Kosugi model. Soil Sci. SS-S-12-00268.

Pollacco, J.A.P., Ugalde, J.M.S., Angulo-Jaramillo, R., Braud, I., Saugier, B., 2008. A Linking Test to reduce the number of hydraulic parameters necessary to simulate groundwater recharge in unsaturated soils. Adv. Water Resour. 31, 355–369. doi:10.1016/j.advwatres.2007.09.002.

Pollacco, J.A.P., Webb, T., McNeill, S., Hu, W., Carrick, S., Hewitt, A., Lilburne, L., 2017. Saturated hydraulic conductivity model computed from bimodal water retention curves for a range of New Zealand soils. Hydrol. Earth Syst. Sci. 21, 2725–2737. doi:10.5194/hess-21-2725-2017.

Rijkse, W.C. (Ed.), 1985. Soil Groups of New Zealand. Part 8, Recent soils. New Zealand Society of Soil Science, Lower Hutt, New Zealand, p. 44.

Schmidt, J., Almond, P.C., Basher, L., Carrick, S., Hewitt, A.E., Lynn, I.H., Webb, T.H., 2005. Modelling loess landscapes for the South Island, New Zealand, based on expert knowledge. N. Z. J. Geol. Geophys. 48, 117–133. doi:10.1080/00288306.2005.9515103.

Tuller, M., Or, D., Dudley, L.M., 1999. Adsorption and capillary condensation in porous media: liquid retention and interfacial configurations in angular pores. Water Resour. Res. 35, 1949–1964. doi:10.1029/1999WR900098.

van Genuchten, M.T., 1980. A closed-form equation for predicting the hydraulic conductivity of unsaturated soils. Soil Sci. Soc. Am. J. 44, 892–898.

van Looy, K., Bouma, J., Herbst, M., Koestel, J., Minasny, B., Mishra, U., Montzka, C., Nemes, A., Pachepsky, Y.A., Padarian, J., Schaap, M.G., Tóth, B., Verhoef, A., Vanderborght, J., van der Ploeg, M.J., Weihermüller, L., Zacharias, S., Zhang, Y., Vereecken, H., 2017. Pedotransfer functions in earth system science: challenges and perspectives: PTFs in earth system science perspective. Rev. Geophys. 55, 1199–1256. doi:10.1002/2017RG000581.

Yang, Y., Wang, L., Wendroth, O., Liu, B., Cheng, C., Huang, T., Shi, Y., 2019. Is the laser diffraction method reliable for soil particle size distribution analysis? Soil Sci. Soc. Am. J. 83, 276–287. doi:10.2136/sssaj2018.07.0252.

Zhuang, J., Jin, Y., Miyazaki, T., 2001. Estimating water retention characteristic from soil particle-size distribution using a non-similar media concept. Soil Sci. 166, 308–321.